Supplemental information
Enhancing Sensitivity of Lateral Flow Assay with Application to SARS-CoV-2

Tao Peng,[1] Xiangpei Liu,[1,2] L. Garry Adams,[1] Girish S. Agarwal,[1] Bruce L. Akey,[1] Jeffrey D. Cirillo,[1] Volker Deckert,[1,3,4] Sahar Delfan,[1] Edward S. Fry,[1] Zehua Han,[1] Philip Hemmer,[1] George W. Kattawar,[1] Moochan Kim,[1] Ming-Che Lee,[1] Chaoyang Lu,[2] Jon Mogford,[1] Reed Nessler,[1] Ben Neuman,[1] Xiaoyu Nie,[1,5] Jianwei Pan,[2] Jane H. Pryor,[1] Navid Rajil,[1] Yanhua Shih,[6] Alexei Sokolov,[1] Anatoly Svidzinsky,[1] Dawei Wang,[7] Zhenhuan Yi,[1] Aleksei Zheltikov,[1,8] and Marlan O. Scully[1,9,10,a)]

[1)] *Texas A&M University, College Station, TX 77843, United States*[b)]
[2)] *University of Science and Technology of China, Hefei 230026, China*
[3)] *Leibniz Institute of Photonic Technology, 07745 Jena, Germany*
[4)] *Friedrich-Schiller-University Jena, Helmholtzweg 4, 07743 Jena, Germany*
[5)] *Xi'an Jiaotong University, Xi'an, Shaanxi 710049, China*
[6)] *University of Maryland, Baltimore County, Baltimore, MD 21250, United States*
[7)] *Zhejiang University, Hangzhou 310027, China*
[8)] *Moscow State University, Moscow 119992, Russia*
[9)] *Baylor University, Waco, TX 76798, United States*
[10)] *Princeton University, Princeton, NJ 08544, United States*

SUPPLEMENT A: SCATTERING FROM NC MEMBRANE

In order to gain insight into the workings of the highly scattering NC membrane, we adopt a simple one-dimensional model that describes light propagating (along the z-axis) in a conservative medium (absorption here is taken to be zero). Within this model, the intensities of the forward- and backward-propagating light waves, $I_f(z)$ and $I_b(z)$, respectively, are coupled by a phase-independent uniform backscattering coefficient ($B\sigma n = \text{constant}$):

$$\frac{\mathrm{d}I_f}{\mathrm{d}z} = \frac{\mathrm{d}I_b}{\mathrm{d}z} = \frac{1}{2}\frac{\mathrm{d}}{\mathrm{d}z}(I_f + I_b) = -B\sigma n(I_f - I_b).$$

(Note: n here is the density of the scatterers, not the absorbing particles.) Since

$$\frac{\mathrm{d}I_f}{\mathrm{d}z} - \frac{\mathrm{d}I_b}{\mathrm{d}z} = 0 \Rightarrow I_f - I_b = \text{constant} = I_{\text{transmitted}},$$

we obtain the solution $I_f(z) = I_0 - B\sigma n z I_{\text{transmitted}}$ and hence

$$I_{\text{transmitted}} = I_0 - B\sigma n Z I_{\text{transmitted}} = \frac{I_0}{1 + B\sigma n Z},$$

where I_0 is the input intensity and Z is the thickness. The corresponding reflection is

$$R = \frac{I_0 - I_{\text{transmitted}}}{I_0} = \frac{B\sigma n Z}{1 + B\sigma n Z} = \frac{B\tau}{1 + B\tau}.$$

SUPPLEMENT B: SCATTERING OF ELECTROMAGNETIC WAVES FROM TWO CONCENTRIC SPHERES

Here we consider a plane wave of frequency ω incident upon a sphere of radius a with a concentric spherical shell of radius $b > a$. The refractive indices of the sphere and the shell are n_1 and n_2 respectively. The refractive index of the outer region is n_3. The corresponding magnetic and dielectric constants are μ_1, μ_2, μ_3 and ε_1, ε_2, ε_3.

The amplitude coefficients for the field expansion over the multipole mode functions are obtained by applying the boundary conditions for the electromagnetic field at the two surfaces of dielectric discontinuity. According to Ref.[1], the total scattering

[a)] scully@tamu.edu

[b)] T. P. and X. L. contributed equally to this work.

cross section of the two concentric spheres is given by a sum over multipoles

$$\sigma_{\text{sca}} = \frac{2\pi c^2}{n_3^2\omega^2}\sum_{n=1}^{\infty}(2n+1)\left(|a_n|^2+|b_n|^2\right), \quad \text{(S.1)}$$

where

$$b_n = -\frac{\frac{\psi_n'(z_{3b})}{z_{3b}}A_1 + \sqrt{\frac{\varepsilon_3}{\mu_3}}j_n(z_{3b})A_2}{\frac{\zeta_n'(z_{3b})}{z_{3b}}A_1 + \sqrt{\frac{\varepsilon_3}{\mu_3}}h_n^{(2)}(z_{3b})A_2},$$

$$a_n = -\frac{j_n(z_{3b})A_3 + \sqrt{\frac{\varepsilon_3}{\mu_3}}\frac{\psi_n'(z_{3b})}{z_{3b}}A_4}{h_n^{(2)}(z_{3b})A_3 + \sqrt{\frac{\varepsilon_3}{\mu_3}}\frac{\zeta_n'(z_{3b})}{z_{3b}}A_4},$$

$\psi_n(z)$ and $\zeta_n(z)$ are the Riccati–Bessel functions,

$$z_{1a} = \frac{\omega n_1}{c}a, z_{2a} = \frac{\omega n_2}{c}a, z_{2b} = \frac{\omega n_2}{c}b, z_{3b} = \frac{\omega n_3}{c}b,$$

and the coefficients $A_1, \ldots, A_4$ are

$$A_1 = \frac{\varepsilon_2}{\mu_2}X + \sqrt{\frac{\varepsilon_1\varepsilon_2}{\mu_1\mu_2}}Y,$$

$$A_2 = \sqrt{\frac{\varepsilon_2}{\mu_2}}Z + \sqrt{\frac{\varepsilon_1}{\mu_1}}W,$$

$$A_3 = \frac{\varepsilon_2}{\mu_2}W + \sqrt{\frac{\varepsilon_1\varepsilon_2}{\mu_1\mu_2}}Z,$$

$$A_4 = \sqrt{\frac{\varepsilon_2}{\mu_2}}Y + \sqrt{\frac{\varepsilon_1}{\mu_1}}X,$$

where

$$X = \frac{\psi_n'(z_{1a})}{z_{1a}}\left[j_n(z_{2b})h_n^{(2)}(z_{2a}) - j_n(z_{2a})h_n^{(2)}(z_{2b})\right],$$

$$Y = j_n(z_{1a})\left[\frac{\psi_n'(z_{2a})}{z_{2a}}h_n^{(2)}(z_{2b}) - \frac{\zeta_n'(z_{2a})}{z_{2a}}j_n(z_{2b})\right],$$

$$Z = \frac{\psi_n'(z_{1a})}{z_{1a}}\left[j_n(z_{2a})\frac{\zeta_n'(z_{2b})}{z_{2b}} - h_n^{(2)}(z_{2a})\frac{\psi_n'(z_{2b})}{z_{2b}}\right],$$
$$W = j_n(z_{1a})\left[\frac{\psi_n'(z_{2b})}{z_{2b}}\frac{\zeta_n'(z_{2a})}{z_{2a}} - \frac{\psi_n'(z_{2a})}{z_{2a}}\frac{\zeta_n'(z_{2b})}{z_{2b}}\right].$$

The prime denotes a derivative with respect to the argument of the Riccati–Bessel function.

We are interested in the limit when the radiation wavelength is much larger than the size of the spheres ($\omega b/c \ll 1$). Using asymptotics of the Riccati–Bessel functions at small argument ($x \ll 1$)

$$\psi_n(x) \approx \frac{2^n n!}{(2n+1)!}x^{n+1},$$

$$\zeta_n(x) \approx \frac{i(2n)!}{2^n n!}\frac{1}{x^n},$$

we obtain that a_n, $b_n \propto (\omega b/c)^{2n+1}$. In particular, for the first two scattering functions we find

$$b_0 \approx i\frac{\omega n_3 b}{c}\left[1 - \frac{\varepsilon_2}{\varepsilon_3}\left(1-\frac{a}{b}\right) - \frac{\varepsilon_1}{\varepsilon_3}\frac{a}{b}\right] - \left(\frac{\omega n_3 b}{c}\right)^2\left[1 - \frac{\varepsilon_2}{\varepsilon_3}\left(1-\frac{a}{b}\right) - \frac{\varepsilon_1}{\varepsilon_3}\frac{a}{b}\right]^2,$$

$$a_0 \approx i\frac{\omega n_3 b}{c}\left[1 - \frac{\mu_2}{\mu_3}\left(1-\frac{a}{b}\right) - \frac{\mu_1}{\mu_3}\frac{a}{b}\right] - \left(\frac{\omega n_3 b}{c}\right)^2\left[1 - \frac{\mu_2}{\mu_3}\left(1-\frac{a}{b}\right) - \frac{\mu_1}{\mu_3}\frac{a}{b}\right]^2,$$

$$b_1 \approx -\frac{2i}{3}\left(\frac{\omega n_3 b}{c}\right)^3\frac{a^3(\varepsilon_1-\varepsilon_2)(\varepsilon_3+2\varepsilon_2) + b^3(\varepsilon_2-\varepsilon_3)(\varepsilon_1+2\varepsilon_2)}{2a^3(\varepsilon_2-\varepsilon_3)(\varepsilon_1-\varepsilon_2) + b^3(\varepsilon_2+2\varepsilon_3)(\varepsilon_1+2\varepsilon_2)}, \quad \text{(S.2)}$$

$$a_1 \approx -\frac{2i}{3}\left(\frac{\omega n_3 b}{c}\right)^3\frac{a^3(\mu_1-\mu_2)(\mu_3+2\mu_2) + b^3(\mu_2-\mu_3)(\mu_1+2\mu_2)}{2a^3(\mu_2-\mu_3)(\mu_1-\mu_2) + b^3(\mu_2+2\mu_3)(\mu_1+2\mu_2)}. \quad \text{(S.3)}$$

Here we used $n_1 = \sqrt{\varepsilon_1\mu_1}$, $n_2 = \sqrt{\varepsilon_2\mu_2}$ and $n_3 = \sqrt{\varepsilon_3\mu_3}$.

The main contribution to the cross section comes from the dipole scattering for which $n = 1$. Plugging Eqs. S.2 and S.3 into Eq. S.1 yields the following answer for the total scattering cross section:

$$\sigma_{\text{sca}} = \frac{8\pi}{3}\left(\frac{\omega n_3}{c}\right)^4 b^6 \left(|F_\varepsilon|^2 + |F_\mu|^2\right), \quad \text{(S.4)}$$

where

$$F_\varepsilon = \frac{f(\varepsilon_1-\varepsilon_2)(\varepsilon_3+2\varepsilon_2)+(\varepsilon_2-\varepsilon_3)(\varepsilon_1+2\varepsilon_2)}{2f(\varepsilon_2-\varepsilon_3)(\varepsilon_1-\varepsilon_2)+(\varepsilon_2+2\varepsilon_3)(\varepsilon_1+2\varepsilon_2)},$$

$$F_\mu = \frac{f(\mu_1-\mu_2)(\mu_3+2\mu_2)+(\mu_2-\mu_3)(\mu_1+2\mu_2)}{2f(\mu_2-\mu_3)(\mu_1-\mu_2)+(\mu_2+2\mu_3)(\mu_1+2\mu_2)},$$

and

$$f = \frac{a^3}{b^3}.$$

The absorption cross section is given by

$$\sigma_{\text{abs}} = \frac{2\pi c^2}{n_3^2\omega^2}\sum_{n=1}^{\infty}(2n+1)\mathrm{Re}\left(a_n + b_n\right),$$

which in the leading order gives

$$\sigma_{\text{abs}} = \frac{4\pi\omega n_3}{c} b^3 \mathrm{Im}\left(F_\varepsilon + F_\mu\right).$$

Introducing diameter of the nanoparticle $d = 2a$, thickness of the protein coating $s = b - a$, and notations $\varepsilon_1 = \epsilon_m$, $\varepsilon_2 = \epsilon_p$, $\varepsilon_3 = \epsilon_l$, we obtain for nonmagnetic spheres with $\mu_1 = \mu_2 = \mu_3 = 1$ the equations given in the main text.

SUPPLEMENT C: EXAMPLES OF QUANTITATIVE LATERAL FLOW ASSAYS AND THEIR ANALYTICAL PARAMETERS

There have been many efforts focused on the enhancement of sensitivity of LFA detection[4,14,15]. High sensitivity LFA detection technologies including optical[5], photoacuostic[16], magnetic[17], and electrochemical methods[18], *etc*. Among all these different approaches, we here summarise and compare our work with other colorimetry methods in the literature in Table S1. We show that our work has reached the lowest quantitative limit of detection as measured by the number concentration of particles. The limit of detection in our work is due to the manufacturing technique of the test strip (the non-specific biochemical binding). To verify this and show the superiority of our detection scheme, in Fig. S1, we examine an idealized experimental model for the LFA. We apply 2 μL of pure (not coated with spike protein) AuNP suspended in water to the nitrocellulose paper (3 mm $\times$ 3 mm). We are able to reach an even better LOD of 1×10^7 particles/μ L, with a contrast of 0.41%. We conclude that in future applications, resolution can likely be further enhanced.

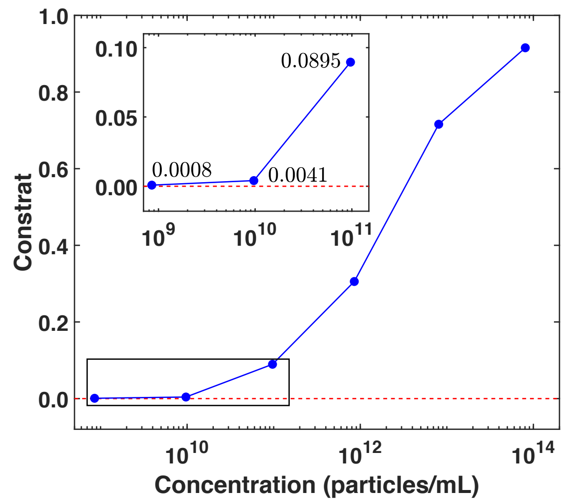

FIG. S1: Contrasts for different pure (not coated with spike protein) AuNP concentration, each sample is 2 μL solution on a 3 mm $\times$ 3 mm area.

[1] A. L. Aden and M. Kerker, "Scattering of electromagnetic waves from two concentric spheres," Journal of Applied Physics **22**, 1242–1246 (1951).

[2] M. Sajid, A.-N. Kawde, and M. Daud, "Designs, formats and applications of lateral flow assay: A literature review," Journal of Saudi Chemical Society **19**, 689–705 (2015).

[3] A. E. Urusov, A. V. Zherdev, and B. B. Dzantiev, "Towards lateral flow quantitative assays: detection approaches," Biosensors **9**, 89 (2019).

[4] V.-T. Nguyen, S. Song, S. Park, and C. Joo, "Recent advances in high-sensitivity detection methods for paper-based

TABLE S1: **Examples of quantitative lateral flow assays and their analytical parameters**[2–4]

Detection	Target analytes	Working range (ng/mL)	Quantitative LOD (number of molecules)
laser readout (the present work)	SARS-CoV-2 IgG antibody	0.1 – 1000	4.01E+08
gold nanoshell colorimetric[5]	Troponin	0.05 – 30	1.67E+09
gold nanopopcorn colorimetric[6]	PCT	0.5 – 10	4.00E+09
commercial detection[7]	Procalcitonin	0.3 – 100	1.25E+10
Silver enhanced colorimetric[8]	PSA	0.1 – 10	2.01E+09
AuNP colorimetric[9]	Human IgG	0.5 – 500	8.02E+8
iridium oxide (IV) NP colorimetric[10]	Human IgG	10 – 1000	2.81E+11
nanofibers colorimetric[11]	Troponin I	0.1 – 10	6.02E+09
smartphone diagnostics unit[12]	C-reactive protein	0.1 – 100	5.01E+8
clinical analysis[13]	Alpha fetoproteins	0 – 150	8.59E+9

lateral-flow assay," Biosensors and Bioelectronics **152**, 112015 (2020).

[5] S. J. Oldenburg, "Increasing the senstivity of lateral flow diagnostic assays with ultra-bright gold nanoshell reporters," Analytical chemistry **76**, 71–79 (2019).

[6] K. Serebrennikova, J. Samsonova, and A. Osipov, "Hierarchical nanogold labels to improve the sensitivity of lateral flow immunoassay," Nano-micro letters **10**, 24 (2018).

[7] J. Szederjesi, E. Almasy, A. Lazar, A. Huțanu, I. Badea, and A. Georgescu, "An evaluation of serum procalcitonin and c-reactive protein levels as diagnostic and prognostic biomarkers of severe sepsis," The Journal of Critical Care Medicine **1**, 147–153 (2015).

[8] M. O. Rodríguez, L. B. Covián, A. C. García, and M. C. Blanco-López, "Silver and gold enhancement methods for lateral flow immunoassays," Talanta **148**, 272–278 (2016).

[9] C. Parolo, A. de la Escosura-Muñiz, and A. Merkoçi, "Enhanced lateral flow immunoassay using gold nanoparticles loaded with enzymes," Biosensors and Bioelectronics **40**, 412–416 (2013).

[10] D. Quesada-González, A. Sena-Torralba, W. P. Wicaksono, A. de la Escosura-Muñiz, T. A. Ivandini, and A. Merkoçi, "Iridium oxide (iv) nanoparticle-based lateral flow immunoassay," Biosensors and Bioelectronics **132**, 132–135 (2019).

[11] W. Kim, S. Lee, and S. Jeon, "Enhanced sensitivity of lateral flow immunoassays by using water-soluble nanofibers and silver-enhancement reactions," Sensors and Actuators B: Chemical **273**, 1323–1327 (2018).

[12] J.-S. Yang, J. Shin, S. Choi, and H.-I. Jung, "Smartphone diagnostics unit (sdu) for the assessment of human stress and inflammation level assisted by biomarker ink, fountain pen, and origami holder for strip biosensor," Sensors and Actuators B: Chemical **241**, 80–84 (2017).

[13] Q. Yang, X. Gong, T. Song, J. Yang, S. Zhu, Y. Li, Y. Cui, Y. Li, B. Zhang, and J. Chang, "Quantum dot-based immunochromatography test strip for rapid, quantitative and sensitive detection of alpha fetoprotein," Biosensors and Bioelectronics **30**, 145–150 (2011).

[14] H. Ye, Y. Liu, L. Zhan, Y. Liu, and Z. Qin, "Signal amplification and quantification on lateral flow assays by laser excitation of plasmonic nanomaterials," Theranostics **10**, 4359 (2020).

[15] J. D. Bishop, H. V. Hsieh, D. J. Gasperino, and B. H. Weigl, "Sensitivity enhancement in lateral flow assays: A systems perspective," Lab on a Chip **19**, 2486–2499 (2019).

[16] S. Li, Y. Zhang, W. Wen, W. Sheng, J. Wang, S. Wang, and J. Wang, "A high-sensitivity thermal analysis immunochromatographic sensor based on au nanoparticle-enhanced two-dimensional black phosphorus photothermal-sensing materials," Biosensors and Bioelectronics **133**, 223–229 (2019).

[17] X.-H. Mu, H.-F. Liu, Z.-Y. Tong, B. Du, S. Liu, B. Liu, Z.-W. Liu, C. Gao, J. Wang, and H. Dong, "A new rapid detection method for ricin based on tunneling magnetoresistance biosensor," Sensors and Actuators B: Chemical **284**, 638–649 (2019).

[18] P. D. Sinawang, L. Fajs, K. Elouarzaki, J. Nugraha, and R. S. Marks, "Tempo-based immuno-lateral flow quantitative detection of dengue ns1 protein," Sensors and Actuators B: Chemical **259**, 354–363 (2018).